

A hybrid-integrated diode laser for the visible spectral range

C.A.A. Franken^{1,†}, A. van Rees^{1,†,*}, Y. Fan¹, D. Geskus², R. Dekker², D.H. Geuzebroek²,
C. Fallnich^{3,1}, P.J.M. van der Slot¹, and K.-J. Boller^{1,3}

¹Laser Physics and Nonlinear Optics Group, Applied Nanophotonics, Faculty of Science and Technology, MESA+ Institute, University of Twente, P.O. Box 217, 7500 AE Enschede, the Netherlands

²LioniX International B.V., P.O. Box 456, 7500 AL Enschede, the Netherlands

³Optical Technologies Group, Institute of Applied Physics, University of Münster, Corrensstraße 2, 48149 Münster, Germany

[†]Both authors contributed equally to this work.

^{*}Corresponding author: a.vanrees@utwente.nl

May 27, 2022

Abstract

Hybrid integrated diode lasers operating in the visible spectrum are of high interest for, *e.g.*, biophotonics and metrology. This type of laser provides single longitudinal mode oscillation with a wide wavelength tunability and a narrow spectral linewidth, by coupling a semiconductor optical amplifier to a micro-ring resonator based photonic circuit. So far, such lasers have only operated at infrared wavelengths. Here we present the first such laser operating in the visible. The laser comprises an AlGaInP gain section coupled to a Si₃N₄ feedback circuit and exhibits a spectral coverage of 10.8 nm around 684.4 nm with up to 4.8 mW output power. The measured intrinsic linewidth is 2.4 ± 0.1 kHz.

1 Introduction

Integration of diode amplifiers in low-loss passive photonic platforms enables highly coherent light sources [1] and provides stability, portability and scalability for optical systems. Especially applications in biophotonics, metrology and quantum computing benefit from these advantages by using photonic integration technology targeted at the visible spectral range, *e.g.*, based on Si₃N₄ material [2, 3]. On-chip, widely tunable and narrowband light sources would be of great benefit for these applications in the visible range. For example, an on-chip laser removes the instability associated with coupling light into photonic circuits in an imaging system for microscopy [4], in implantable neurophotonic probes [5] or in a fluorescence biosensor [6]. Integrated refractive index biosensors [7] particularly benefit from integrated narrow-linewidth sources, because the use of a highly coherent source enhances the resolution of spectral detection, and, hence, lowers the detection limit [8]. Furthermore, compact and frequency-stable light sources in the visible spectral range are required for atom cooling and trapping [9] in portable optical atomic clocks [10] and quantum information processors [11].

Hybrid integration of semiconductor amplifiers with spectrally-selective feedback circuits using low-loss dielectric waveguides results in widely tunable lasers that can be seamlessly integrated in photonic integrated circuits [12]. In addition, these lasers provide single longitudinal mode oscillation with a narrow intrinsic linewidth known as the Schawlow-Townes linewidth [13]. Nevertheless, operation of hybrid and also heterogeneously integrated diode lasers was so far limited to the infrared spectral range, *e.g.*, at 2.6 μm [14], 1.55 μm [1], 1.27 μm [15], 1.06 μm [16], 1.0 μm [17] and 0.85 μm [18].

Although an InGaN-based laser has been integrated on a Si wafer by epitaxial growth [19], integration of a diode laser for visible light in a photonic circuit has not been demonstrated yet. To avoid two-photon absorption, such circuits require transparent dielectric waveguides, *e.g.*, based on TiO₂ or Si₃N₄. In addition, the waveguide should be optimized to reduce scattering loss resulting from roughness of the core-to-cladding interface, which increases strongly towards shorter wavelengths ($\sim 1/\lambda^3$) [20]. Heterogeneous integration, using vertical tapers for evanescent coupling between an

InGaP laser and passive TiO_2 waveguides was investigated [21], but the wafers did not bond due to surface roughness. To date, no successful realization of a hybrid or heterogeneous integrated diode laser for the visible spectral range has been reported.

In this work we demonstrate the first operation of a hybrid integrated diode laser in the visible. Using Si_3N_4 waveguides, we provide a feedback circuit with negligible absorption loss and low scatter loss via a weakly confined optical mode. This novel laser paves the way to on-chip narrow-linewidth light sources in the visible spectral range.

2 Laser design and hybrid integration

The design of the hybrid laser is shown schematically in Fig. 1. The laser cavity is formed by a semiconductor chip coupled to a $\text{Si}_3\text{N}_4/\text{SiO}_2$ based feedback chip. The multiple quantum well AlGaInP semiconductor optical amplifier (SOA, Sacher SAL-0690-25) is 600 μm long and provides a gain bandwidth of approximately 10 nm around 685 nm. Its back facet has a high reflectivity (HR) coating of $\sim 95\%$, which forms one mirror of the laser cavity. The other mirror is a reflective Vernier filter formed by a y-junction and two cascaded microring resonators (MRRs) to provide highly frequency-selective feedback.

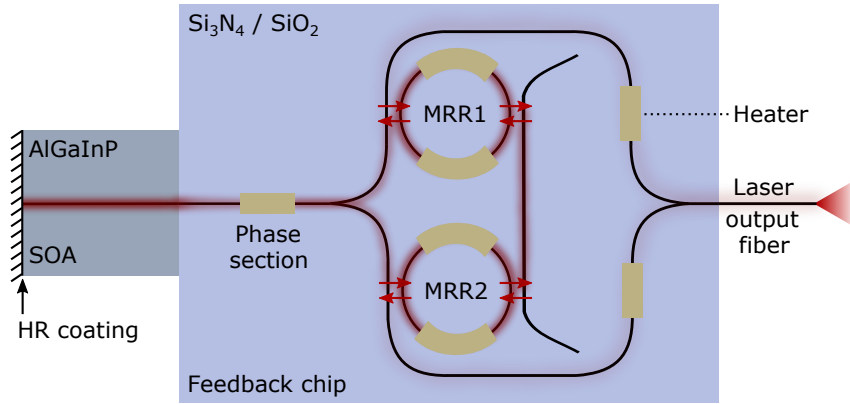


Figure 1: Schematic overview of the hybrid laser comprising an AlGaInP optical amplifier butt-coupled to a $\text{Si}_3\text{N}_4/\text{SiO}_2$ feedback chip. The chip contains two sequential microring resonators (MRR1, MRR2) that form a Vernier filter within a loop mirror. Directional couplers are indicated by red arrows. Heaters (yellow) are placed on the MRRs, on the intracavity phase section and near the output Y-junction.

To minimize propagation losses, the feedback circuit is implemented using a high aspect ratio Si_3N_4 core of 2 μm wide and 25 nm thick buried in a SiO_2 cladding [22, 3]. Key to low propagation loss of this single-transverse-mode waveguide is the small height of the sidewalls to minimize the scattering loss, as the sidewall etching produces a larger interface roughness than the layer deposition process, which defines the top and bottom surface of the waveguide. We characterized the propagation loss to be 0.3 ± 0.2 dB/cm for the TE_{00} mode, based on measuring the insertion loss of 2.4-cm long straight waveguides and subtracting the estimated fiber to chip coupling loss of 1 dB per interface. The smallest bending radius for this waveguide geometry is chosen as 1200 μm to ensure that bend radiation loss is negligible compared to the straight propagation loss. To obtain good modal overlap with a single-mode, polarization-maintaining output fiber (Nufern PM460-HP), the waveguide width is tapered down to 0.8 μm at the output side of the feedback chip, while for good modal overlap with the gain section no taper is required at the gain-side.

The functionality of the feedback circuit is twofold. Frequency filtering is realized using two high-quality ring resonators with slightly different radii. These rings have radii of 1200 and 1205 μm and an estimated Q-factor of $7.3 \cdot 10^5$. The measured Vernier FSR is 9.90 ± 0.05 nm at the nominal wavelength of $\lambda = 685$ nm [12]. This FSR is approximately equal to the gain bandwidth of the SOA. The second function is to lower the intrinsic laser linewidth with a long effective length of the feedback circuit [23]. At resonance, the effective length of each ring is enhanced by a factor of 13.7 to 10.4 cm, which is calculated using the ring radius, the measured power coupling $\kappa^2 = 0.043$ for the symmetric directional couplers between the bus waveguide and ring, and the measured propagation loss. Summing the optical lengths of all elements gives a maximum effective roundtrip length of 39.0 cm for the laser cavity. As the length of the laser cavity is strongly frequency dependent, the cavity modes are non-equidistant with a calculated minimum mode spacing of 1.3 pm (0.81 GHz). Single longitudinal mode oscillation is expected, because this mode spacing is larger than the calculated 0.61 pm (0.39 GHz) full-width-at-half-maximum (FWHM) of the Vernier resonance.

Thermo-optic phase tuning of the feedback circuit is realised via resistive heaters. Tuning the ring heaters is used for wavelength selection, while tuning the intracavity phase section is used to align a cavity resonance with the ring resonances. The light extracted from the cavity is combined using a Y-junction before coupling it into the output fiber. To balance the phase in both extraction paths for maximum output coupling, one or both heaters placed near this Y-junction can be tuned. Introducing a phase shift of 2π with these resistive heaters requires approximately 400 mW of dissipated electrical power.

To enable stable laser operation via hybrid integration, the amplifier, feedback chip and output fiber were all aligned for optimum coupling and bonded with an adhesive. The SOA and heaters were wire bonded to an adapter board for electrical connections. The SOA pump current and heater currents are supplied with a Thorlabs LDC205B current source and a Nicslab XPOW-8AX-CCvCV multi-channel power controller, respectively. The hybrid assembly is placed on a subcarrier with a heat sink, which is temperature-controlled using a Peltier element. For all measurements, as described next, the temperature is set at 20 °C.

3 Experimental results

When pumping the SOA above threshold, scattered light from the feedback chip can be observed. Figure 2 shows a photograph of the assembled laser when pumped at the maximum allowed pump current of 90 mA. This photo demonstrates the first operation of a hybrid integrated diode laser in the visible spectral range. We tuned the phase section to align a cavity resonance with a Vernier resonance of the two rings, which is confirmed by the bright scattered light from both rings. We calculate that for such alignment, only 18% of the light circulating inside the cavity passes the rings towards the output. To extract more light from the cavity, the phase section can be used to slightly detune the cavity resonance away from the ring resonances.

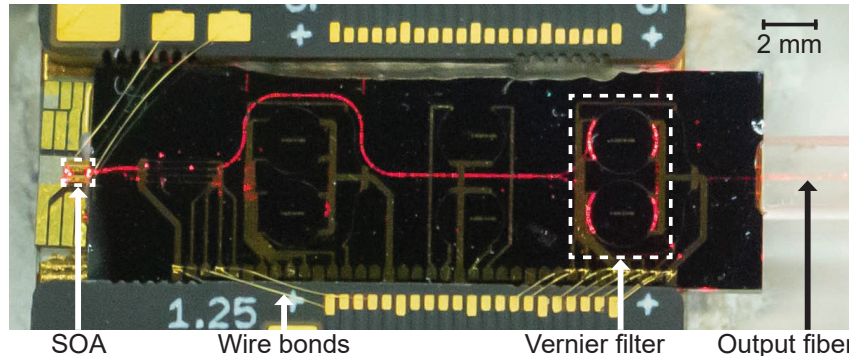


Figure 2: Photograph of the hybrid laser pumped at 90 mA. Bright scattered light from both rings indicates that a cavity mode is tuned to be aligned with the ring resonances.

To measure the laser output power and spectral characteristics, the laser was connected via a 50/50 fiber coupler (Thorlabs TW670R5A2) to a power sensor (Thorlabs S150C) and an optical spectrum analyzer (OSA, ANDO AQ6317). Figure 3(a) shows the measured fiber-coupled output power as function of pump current, corrected for the splitting ratio of the coupler. For each measurement, the heater on the phase section was optimized for maximum output power, while other heaters were not activated. Figure 3(a) indicates a threshold current of 46 mA. Above threshold, the output power increases approximately linearly with a slope efficiency of 0.11 mW/mA, indicated with the linear fit line through all points except the four low outliers. These outliers were likely caused by spectral mode hops, since current-induced refractive index changes of the SOA caused the laser to hop to modes that were less efficiently coupled out. We measured a maximum output power of 4.8 mW at the maximum current of 90 mA. For this setting, we also measured the laser's spectral characteristics with the OSA using a 0.01 nm resolution bandwidth. This spectrum, as shown in Fig. 3(b), reveals a single-wavelength peak at 683.9 nm with a high signal-to-noise ratio of 40 dB. However, as the resolution bandwidth of the OSA is insufficient to distinguish adjacent cavity modes, additional measurements are described that confirm single-mode oscillation.

To determine the spectral coverage of the laser, we varied the electrical power to the heater on MRR1. This shifts the resonant frequency of the underlying ring, thereby changing the Vernier feedback frequency. Fig. 4(a) shows several superimposed laser spectra as measured with the OSA and at a 50-mA pump current. The phase section and a heater near the output Y-junction were optimized for each measurement to obtain single-wavelength laser emission with high output coupling. We observe that the laser wavelength can be tuned over a range of 10.8 nm around 684.4 nm, which

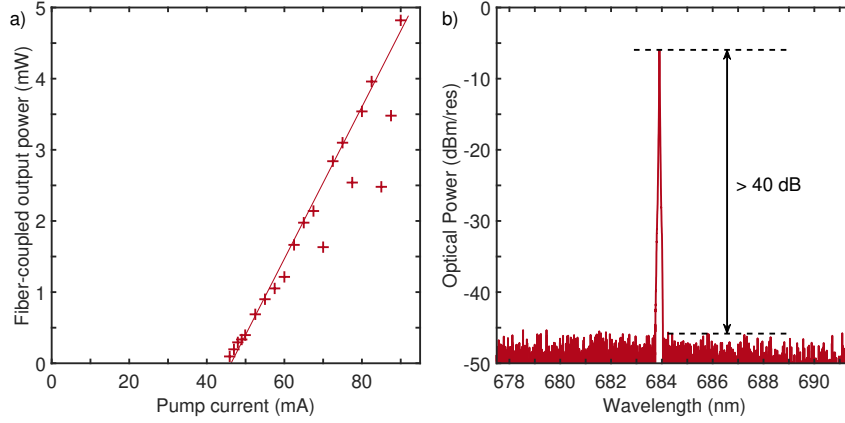


Figure 3: a) Fiber-coupled output power versus pump current, with optimization of the phase section heater. b) Optical power spectrum measured for a pump current of 90 mA.

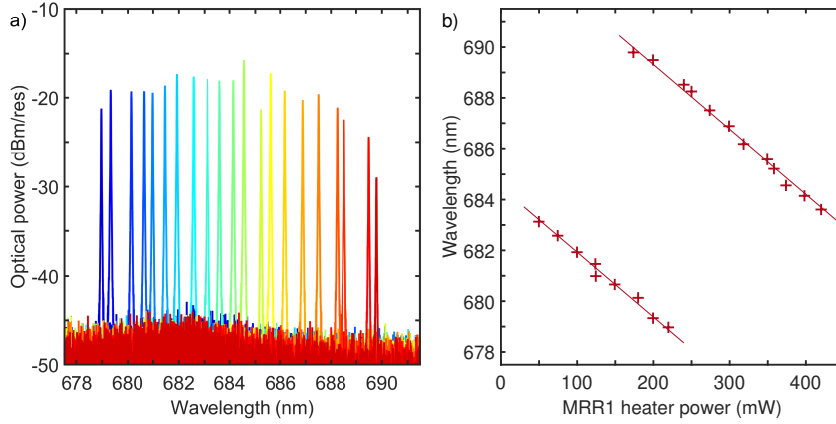


Figure 4: a) Superimposed laser spectra of the hybrid integrated laser, as measured with an OSA set to 0.01 nm resolution and obtained by varying the heater power to MRR1. b) Peak laser wavelength extracted from the laser spectra in a) as function of heater power.

coincides well with the specified gain bandwidth of the amplifier. The highest output power was measured near the peak of the gain spectrum, as expected. For a better qualification of laser tuning, Fig. 4(b) shows the extracted peak wavelengths as function of the heater power at MRR1. The laser wavelength decreases approximately linearly with increasing heater power, except for large hops when the laser is operated near the edge of the gain bandwidth. We fitted two parallel lines through the data points to retrieve the hop distance. The wavelength spacing between these lines is 9.9 nm, which agrees well with the separately measured FSR of the solitary Vernier filter.

To verify that optimized heater settings provide oscillation in a single longitudinal mode, *i.e.*, to spectrally resolve also adjacent longitudinal modes, we used a setup to detect the beating of laser modes in the radio frequency (RF) domain. For this purpose, the laser output was sent to a fast photodiode (Thorlabs DXM12CF) and an RF spectrum analyzer (RFSA, Agilent E4405B). The RFSA was set to a resolution bandwidth of 1 MHz, and swept over a range up to 8 GHz, which would be sufficient to detect the beating between multiple longitudinal modes within a single Vernier resonance. We emphasize that the RF range is wider than the 0.01 nm (6 GHz) resolution bandwidth of the OSA, which ensures that multiple mode oscillations would be noticed. Figure 5 shows an example of the recorded optical (a) and RF (b) spectra, when the laser was optimized for single longitudinal mode oscillation. This optical spectrum shows a single wavelength, while the corresponding RF spectrum shows no indication of the presence of any beat frequencies. We note that the RF spectrum showed several beat frequencies with arbitrary settings of the laser. The RF and optical spectra combined allow us to conclude that the laser can oscillate in a single longitudinal mode with a side mode suppression ratio of at least 39 dB.

To determine the intrinsic linewidth of the laser, the output was sent through an isolator (Thorlabs IO-F-690APC) to a delayed self-heterodyne detection setup. The setup uses a fiber-based Mach-Zehnder interferometer, where one arm contains a 200 MHz acousto-optic modulator (AA Opto-Electronic MT200-R18-FIO-SM0 with MODA200-D2-34 driver), while the other arm contains a 1-

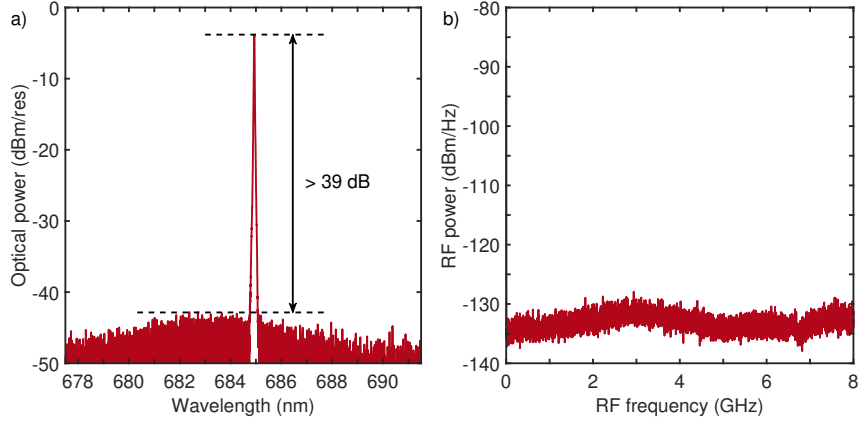


Figure 5: Optical spectrum (a) and RF spectrum (b) of the laser output with the laser optimized for single longitudinal mode oscillation. The pump current was set to 90 mA.

km long single-mode fiber as a delay (Thorlabs SM600), limited in length by the relatively high propagation loss of 6 dB/km. The beat signal at the output was recorded using the fast photodiode connected to the RFSA, set to a radio and video bandwidth of 10 kHz, and averaged over 50 sweeps. Fig. 6 shows the measured power spectrum of the beat signal as the blue trace. For this measurement, the pump current was supplied by a battery-operated current source (ILX Lightwave LDX-3620) set to the maximum allowed value of 90 mA. We tuned MRR2 to set the laser’s wavelength near maximum gain at 685.6 nm and fine-tuned the phase section to minimize the intrinsic linewidth. The recorded RF signal was well above the noise floor of the setup, displayed as the grey trace, which we measured with the laser turned off. In the blue trace, periodic modulations of 200 kHz can be observed, in consistency with the 1-km fiber delay and an even longer coherence length of the laser [24]. By fitting this trace to a Gaussian profile, as shown with the green curve, we find a FWHM linewidth of 56.3 ± 0.4 kHz. This FWHM linewidth of the free-running laser is mainly caused by technical noise sources and can be reduced by locking the laser frequency to a high-finesse cavity or a Sr transition [9]. To obtain an estimation of the intrinsic linewidth, we fitted the recorded signal to a Lorentz function, multiplied by periodic modulations (Eq. 6 from [24]), as shown with the red curve. The fitted Lorentzian linewidth is 2.4 ± 0.1 kHz, which confirms that the laser has a very narrow intrinsic linewidth.

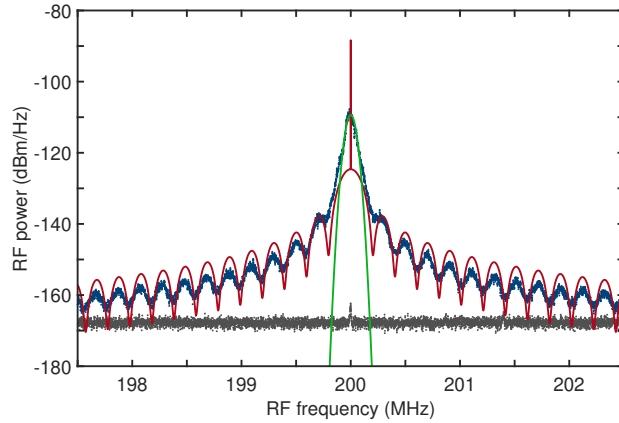


Figure 6: Recorded beat signal (blue trace) and background (grey trace) from the delayed self-heterodyne measurement setup, together with a fitted Gaussian profile (green curve) and a fitted modulated Lorentz profile (red curve).

4 Conclusions

Here, we demonstrate the realization of the first hybrid integrated diode laser in the visible spectral range. The maximum output power is 4.8 mW for a pump current of 90 mA and the spectral coverage amounts to 10.8 nm around 684.4 nm. The hybrid integration of an AlGaInP optical amplifier with a

Si₃N₄ feedback chip, used for sharp Vernier filtering with high-quality microring resonators, enables single longitudinal mode laser oscillation. The long effective optical cavity roundtrip length of up to 39.0 cm provides a narrow intrinsic linewidth of down to 2.4 ± 0.1 kHz. Improving the laser design, *e.g.*, by adding an intracavity tunable coupler for the extraction of the output power independent from the frequency filtering [12], would improve overall performance of the laser, including higher output power and lower intrinsic linewidth. The concept of hybrid integrated diode lasers with very small intrinsic linewidth could possibly cover the whole visible spectral range. Realization of a fully integrated multi-color visible laser engine [25] would then become feasible for numerous applications.

Funding

European Union’s Horizon 2020 research and innovation program (688519, PIX4life).

Acknowledgments

The authors would like to thank R. Heuvink for support with the feedback circuit characterization.

Disclosures

The authors declare no conflict of interest.

References

- [1] Y. Fan, A. van Rees, P. J. M. van der Slot, J. Mak, R. M. Oldenbeuving, M. Hoekman, D. Geskus, C. G. H. Roeloffzen, and K.-J. Boller, “Hybrid integrated InP-Si₃N₄ diode laser with a 40-Hz intrinsic linewidth,” *Opt. Express* **28**, 21713–21727 (2020).
- [2] P. Muñoz, P. W. L. van Dijk, D. Geuzebroek, M. Geiselmann, C. Domínguez, A. Stassen, J. D. Doménech, M. Zervas, A. Leinse, C. G. H. Roeloffzen, B. Gargallo, R. Baños, J. Fernández, G. M. Cabanes, L. A. Bru, and D. Pastor, “Foundry developments toward silicon nitride photonics from visible to the mid-infrared,” *IEEE J. Sel. Top. Quantum Electron.* **25**, 8200513 (2019).
- [3] M. A. Porcel, A. Hinojosa, H. Jans, A. Stassen, J. Goyvaerts, D. Geuzebroek, M. Geiselmann, C. Dominguez, and I. Artundo, “Silicon nitride photonic integration for visible light applications,” *Opt. & Laser Technol.* **112**, 299 – 306 (2019).
- [4] J.-C. Tinguely, Ø. I. Helle, and B. S. Ahluwalia, “Silicon nitride waveguide platform for fluorescence microscopy of living cells,” *Opt. Express* **25**, 27678–27690 (2017).
- [5] W. D. Sacher, X. Luo, Y. Yang, F.-D. Chen, T. Lordello, J. C. C. Mak, X. Liu, T. Hu, T. Xue, P. Guo-Qiang Lo, M. L. Roukes, and J. K. S. Poon, “Visible-light silicon nitride waveguide devices and implantable neurophotonic probes on thinned 200 mm silicon wafers,” *Opt. Express* **27**, 37400–37418 (2019).
- [6] L. Liu, D. Shan, X. Zhou, H. Shi, B. Song, F. Falke, A. Leinse, and R. Heideman, “TriPleX™ waveguide-based fluorescence biosensor for multichannel environmental contaminants detection,” *Biosens. Bioelectron.* **106**, 117–121 (2018).
- [7] K. E. Zinoviev, A. B. Gonzalez-Guerrero, C. Dominguez, and L. M. Lechuga, “Integrated bimodal waveguide interferometric biosensor for label-free analysis,” *J. Light. Technol.* **29**, 1926–1930 (2011).
- [8] I. M. White and X. Fan, “On the performance quantification of resonant refractive index sensors,” *Opt. Express* **16**, 1020–1028 (2008).
- [9] C. Qiao, C. Z. Tan, F. C. Hu, L. Couturier, I. Nosske, P. Chen, Y. H. Jiang, B. Zhu, and M. Weidemüller, “An ultrastable laser system at 689 nm for cooling and trapping of strontium,” *Appl. Phys. B* **125**, 215 (2019).
- [10] N. Poli, M. Schioppo, S. Vogt, S. Falke, U. Sterr, C. Lisdat, and G. M. Tino, “A transportable strontium optical lattice clock,” *Appl. Phys. B* **117**, 1107–1116 (2014).
- [11] K. K. Mehta, C. Zhang, M. Malinowski, T.-L. Nguyen, M. Stadler, and J. P. Home, “Integrated optical multi-ion quantum logic,” *Nature* **586**, 533–537 (2020).
- [12] K.-J. Boller, A. van Rees, Y. Fan, J. Mak, R. E. M. Lammerink, C. A. A. Franken, P. J. M. van der Slot, D. A. I. Marpaung, C. Fallnich, J. P. Epping, R. M. Oldenbeuving, D. Geskus, R. Dekker, I. Visscher, R. Grootjans, C. G. H. Roeloffzen, M. Hoekman, E. J. Klein, A. Leinse, and R. G. Heideman, “Hybrid integrated semiconductor lasers with silicon nitride feedback circuits,” *Photonics* **7**, 4 (2019).

- [13] A. L. Schawlow and C. H. Townes, “Infrared and optical masers,” *Phys. Rev.* **112**, 1940–1949 (1958).
- [14] S.-P. Ojanen, J. Viheriälä, M. Cherchi, N. Zia, E. Koivusalo, P. Karioja, and M. Guina, “GaSb diode lasers tunable around 2.6 μm using silicon photonics resonators or external diffractive gratings,” *Appl. Phys. Lett.* **116**, 081105 (2020).
- [15] T. Komljenovic, S. Srinivasan, E. Norberg, M. Davenport, G. Fish, and J. E. Bowers, “Widely tunable narrow-linewidth monolithically integrated external-cavity semiconductor lasers,” *IEEE J. Sel. Top. Quantum Electron.* **21**, 1501909 (2015).
- [16] J. T. Bovington, M. J. R. Heck, and J. E. Bowers, “Heterogeneous lasers and coupling to Si_3N_4 near 1060 nm,” *Opt. Lett.* **39**, 6017–6020 (2014).
- [17] Y. Zhu and L. Zhu, “Narrow-linewidth, tunable external cavity dual-band diode lasers through InP/GaAs- Si_3N_4 hybrid integration,” *Opt. Express* **27**, 2354–2362 (2019).
- [18] S. Kumari, J. Gustavsson, E. P. Haglund, J. Bengtsson, A. Larsson, G. Roelkens, and R. Baets, “Design of an 845-nm GaAs vertical-cavity silicon-integrated laser with an intracavity grating for coupling to a SiN waveguide circuit,” *IEEE Photonics J.* **9**, 1504109 (2017).
- [19] Y. Sun, K. Zhou, Q. Sun, J. Liu, M. Feng, Z. Li, Y. Zhou, L. Zhang, D. Li, S. Zhang, M. Ikeda, S. Liu, and H. Yang, “Room-temperature continuous-wave electrically injected InGaN-based laser directly grown on Si,” *Nat. Photonics* **10**, 595–599 (2016).
- [20] D. Melati, F. Morichetti, and A. Melloni, “A unified approach for radiative losses and backscattering in optical waveguides,” *J. Opt.* **16**, 055502 (2014).
- [21] T. Kamei, T. Kamikawa, M. Araki, S. P. DenBaars, S. Nakamura, and J. E. Bowers, “Research toward a heterogeneously integrated InGaN laser on silicon,” *Phys. Status Solidi A* **217**, 1900770 (2020).
- [22] C. G. H. Roeloffzen, M. Hoekman, E. J. Klein, L. S. Wevers, R. B. Timens, D. Marchenko, D. Giskus, R. Dekker, A. Alippi, R. Grootjans, A. van Rees, R. M. Oldenbeuving, J. P. Epping, R. G. Heideman, K. Wörhoff, A. Leinse, D. Geuzebroek, E. Schreuder, P. W. L. van Dijk, I. Visscher, C. Taddei, Y. Fan, C. Taballione, Y. Liu, D. Marpaung, L. Zhuang, M. Benelajla, and K. Boller, “Low-loss Si_3N_4 TriPleX optical waveguides: Technology and applications overview,” *IEEE J. Sel. Top. Quantum Electron.* **24**, 4400321 (2018).
- [23] B. Liu, A. Shakouri, and J. E. Bowers, “Passive microring-resonator-coupled lasers,” *Appl. Phys. Lett.* **79**, 3561–3563 (2001).
- [24] L. Richter, H. Mandelberg, M. Kruger, and P. McGrath, “Linewidth determination from self-heterodyne measurements with subcoherence delay times,” *IEEE J. Quantum Electron.* **22**, 2070–2074 (1986).
- [25] A. Mashayekh, T. Klos, S. Koch, F. Merget, D. Geuzebroek, E. Klein, T. Veenstra, M. Büscher, P. Leisching, and J. Witzens, “Miniaturized PIC multi-color laser engines for the life sciences,” in *Proceedings Volume 10922, Smart Photonic and Optoelectronic Integrated Circuits XXI*, 109221U (SPIE, 2019).